*Laser and Particle Beams* (2006), *24*, 217–222. Printed in the USA.

DOI: 10.1017/S0263034606060319

# Simulations of heating of solid targets by fast electrons

J. J. HONRUBIA, C. ALFONSÍN, L. ALONSO, B. PÉREZ, AND J. A. CERRADA
ETSII, Universidad Politécnica, Madrid, Spain

(RECEIVED 11 November 2005; ACCEPTED 22 December 2005)

**Abstract**

Recent experiments of fast electron heating of aluminum foil targets have been analyzed by means of hybrid PIC simulations. A suitable initial angular distribution of fast electrons has been used and the diameter of the fast electron source has been fitted to reproduce with the same simulation parameters the beam divergence, $K_\alpha$ yields and temperatures at the target rear surface measured in the experiments. This results in a consistent description of the fast electron propagation that can be useful in general for simulations of laser-driven fast electron transport in dense media.

**Keywords:** Fast ignition; Laser-driven fast electron transport; Ultra-high intensity laser interaction

## 1. INTRODUCTION

Laser-driven fast electron transport in solid targets has been studied by experiments (Baton *et al*., 2003; Key *et al*., 2004; Koch *et al*., 2001; Kodama *et al*., 2001; Roth *et al*., 2005; Santos *et al*., 2002; Stephens *et al*., 2004), theory (Fill, 2001; Tikhonchuk, 2002), and simulations (Bell & Kingham, 2003; Bibi *et al*., 2004; Davies, 2002; Gremillet *et al*., 2002, Honrubia *et al*., 2005). Experiments have shown the propagation of fast electrons with a relatively large divergence, that is, within a cone angle of 40° (Key *et al*., 2004; Stephens *et al*., 2004). However, the hybrid PIC codes developed to simulate these experiments does not reproduce this divergence when standard simulation parameters are used (Stephens *et al*., 2004). Therefore, the capability of these codes to simulate fast electron transport in large scale dense plasmas has not been fully exploited until now. Here, we found that the initial electron angular distribution is very important to put hybrid PIC simulations closer to experiments.

We focused our study on recent experiments of heating aluminum foil targets by fast electrons (Key *et al*., 2004; Stephens *et al*., 2004; Martinolli *et al*., 2004). Previous calculations (Honrubia *et al*., 2004) have shown temperatures at the target rear surface to be two or three times higher than measurements (Key *et al*., 2004). These differences can be explained by the excessive beam collimation typically found in hybrid PIC codes, which relies on the initial angular distribution used for fast electrons (Bell & Kingham, 2003; Honrubia *et al*., 2005). Here, we used a suitable angular distribution based on the ejection angle of ponderomotively accelerated electrons in order to reproduce the temperatures, $K_\alpha$ yields and effective propagation angles measured in those experiments. This distribution has also been used by Stephens *et al*. (2004) in the context of the Monte Carlo collisional simulations and by Alonso (2003) in the context of hybrid PIC simulations. With such a distribution, low energy electrons are injected into the simulation box with large divergence angles while high energy electrons are injected within a cone half-angle of 20°–30° as in standard hybrid calculations (Davies, 2002). This energy-dependent initial divergence of fast electrons was evidenced in experiments by Gremillet *et al*. (1999), and has been recently included in simulations by Evans *et al*. (2005), and Town *et al*. (2005) by adding a constant thermal spread to the forward momentum distribution of fast electrons.

This paper is organized as follows. In Section 2, we briefly present the simulation model used. In Section 3, we describe the experiment analyzed, the parameters used in simulations, and the results obtained. Finally, the conclusions and future developments are summarized in Section 4.

## 2. SIMULATION MODEL

Simulations have been carried out with the hybrid PIC code described in Honrubia *et al*. (2004, 2005) run in two-dimensional r-z cylindrical geometry mode. Fast electrons are injected in the simulation box with Gaussian distributions in radius and time, and an exponential distri-

Address correspondence and reprint requests to: J.J. Honrubia, ETSII, Universidad Politécnica de Madrid, José Gutiérrez Abascal 2, 28006-Madrid, Spain. E-mail: javier.honrubia@upm.es

bution in energy. Temperatures of this last distribution are computed by means of the ponderomotive scaling formula $kT_f = m_e c^2[(1 + I_{18}\lambda_\mu^2/1.37)^{1/2} - 1]$ (Wilks *et al*., 1992), where $T_f$ is the fast electron temperature, $I_{18}$ is the laser intensity in units of $10^{18}$ W/cm$^2$, $\lambda_\mu$ is the wavelength in microns, and $m_e$ is the electron rest mass. Fast electron angular distribution is given by the energy-dependent ejection angle of ponderomotively accelerated electrons, $\theta_f = \tan^{-1}[(2/(\gamma - 1))^{1/2}]$ (Quesnel & Mora, 1998), where $\gamma$ is the relativistic Lorentz factor, in such a manner that fast electrons are injected with an angle uniformly distributed between 0 and $\theta_f$. Notice that the energy dependence of the cone half-angle $\theta_f$ through $\gamma$ leads to an almost isotropic electron distribution at low energies, and to a highly forward peaked distribution at high energies. Notice also that the $\gamma$ factor depends on the radial coordinate and time by means of the Gaussian distributions of the laser intensity assumed.

The ejection angle formula combined with the Gaussian distributions of the fast electron pulse in radius and time gives the overall initial angular distribution shown in Figure 1 for the laser pulse parameters used in this paper. Notice that this distribution is far from the Gaussian one, showing a plateau up to 20° and a FWHM (full width at half maximum) of, approximately, 40°, much higher than the typical 20°–30° divergences used in "standard" hybrid simulations. The top-hat angular distribution used by Davies (2002) is also shown for comparison.

Resistivities are computed as in the model of Eidmann *et al*. (2000) assuming separate temperatures for electron and ion species. Tables generated by MPQeos (Kemp & Meyer-ter-Vehn, 1998) are used to obtain temperatures and ionization of the background plasma from Coulomb energy deposition and Ohmic heating due to the return current.

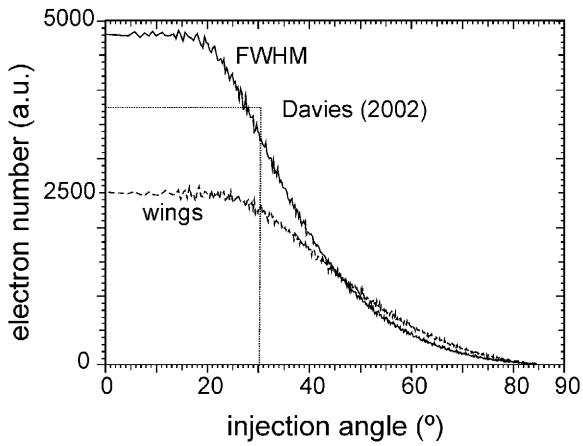


**Fig. 1.** Overall angular distribution of the fast electrons injected in the simulation box with the laser pulse parameters described in Section 3. The curve labeled with FWHM corresponds to electrons injected within the FWHM of the Gaussian distribution in radius, while the curve labeled by wings corresponds to electron injected at larger radii. The distribution used by Davies (2002) for all electrons is also shown.

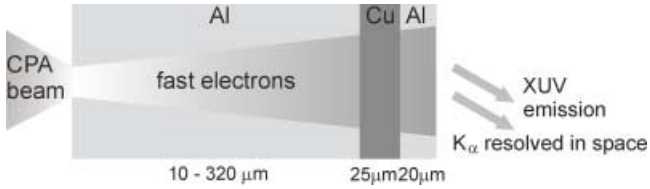


**Fig. 2.** Targets used in the fast electron heating experiments analyzed in this paper (Key *et al*., 2004; Stephens *et al*., 2004).

The numerical parameters used are a time step of 1.5 fs and a cell width of 0.5 $\mu$m in both axial and radial directions. $10^6$ particles are injected in 2 ps, with a peak rate of 1450 particles per time step at 1 ps. Fast electrons are reflected at the front and rear surfaces to simulate the refluxing or recirculation of fast electrons within the target.

## 3. RESULTS

The targets analyzed consist of an aluminum transport layer with thickness ranging from 10 to 320 $\mu$m, followed by a 25 $\mu$m copper layer to absorb radiation coming from the laser interaction region, and a 20 $\mu$m aluminum fluor layer, as depicted in Figure 2 (Key *et al*., 2004; Stephens *et al*., 2004). These targets were illuminated by a CPA laser beam focused onto a 10 $\mu$m diameter spot (FWHM), with a mean irradiance at FWHM of $2.5 \times 10^{19}$ W/cm$^2$ and a pulse duration of 1 ps (FWHM). The mean kinetic energy of fast electrons is 1.5 MeV (FWHM) and the laser-to-fast-electron conversion efficiency is assumed to be 33%. The diagnostics used were $K_\alpha$ spectroscopy of the aluminum fluor layer resolved in space and thermal self-emission to measure the temperature distribution at the target rear surface.

In the next Sections, we first analyze the effective propagation angle and fit the size of the fast electron source to reproduce as much as possible the size of the $K_\alpha$ distribution at the rear surface of the target. We then check the attenuation of the $K_\alpha$ yield with target thickness and the temperature distribution at the target rear side. Our goal was to reproduce the measurements of these three diagnostics with the same set of simulation parameters.

### 3.1. Effective propagation angle

Propagation of fast electrons in solid targets depends strongly on their initial angular distribution. If the standard Gaussian distribution with a FWHM of 20° is used, previous simulations of the experiments considered in this paper have shown that the beam is resistively collimated by the self-generated azimuthal magnetic field along distances of, approximately, 150 $\mu$m (Honrubia *et al*., 2004). This result agrees with the analytical model developed by Bell and Kingham (2003), which predicts beam collimation for the electron beam parameters shown above. It does not agree, however, with the experimental results reported by Stephens *et al*.

https://doi.org/10.1017/S0263034606060319 Published online by Cambridge University Press

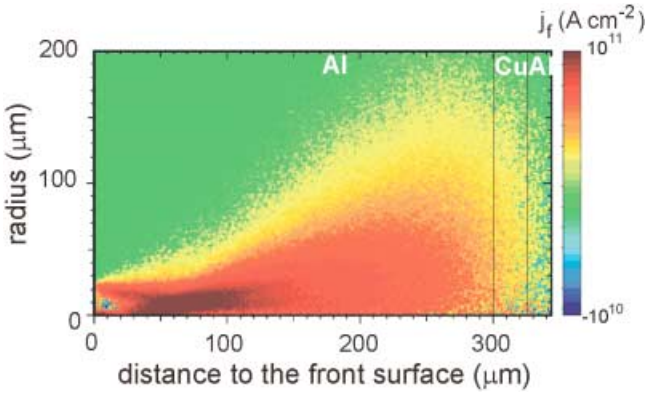


**Fig. 3.** Fast electron current density in the 300 $\mu$m Al target shown in Figure 2. Fast electrons are injected at the left of the simulation box.

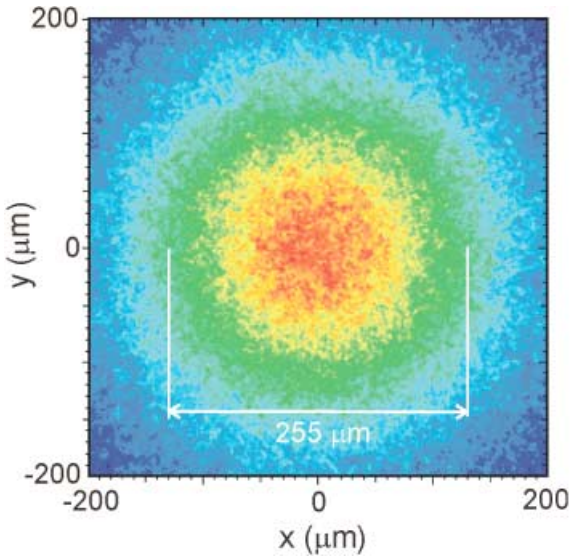


**Fig. 4.** Computed $K_\alpha$ image at the rear surface of the 300 $\mu$m target shown in Figure 2.

(2004), which clearly show that electrons propagate in the target with an effective cone angle of 40° rather than within a cylinder with a diameter of the order of the laser focal spot.

We used the energy-dependent angular distribution discussed in Section 2 and shown in Figure 1 to simulate fast electron propagation in the target. With this distribution, the fast electron current density spreads strongly when electrons penetrate the target, resulting in a lower current density and field generation. This in turn leads to the beam collimation over a shorter distance, 60–70 $\mu$m, than that found in standard hybrid PIC simulations (150 $\mu$m), as depicted in Figure 3. For higher penetrations, the self-generated fields have a decreasing importance, and fast electron transport is mainly dominated by the angular spread with which fast electrons come out from the collimated region, and by Coulomb collisions with the background plasma. The map of the computed $K_\alpha$ distribution for the 300 $\mu$m target is depicted in Figure 4, where the diameter of the $K_\alpha$ spot shown corresponds to an effective propagation angle of 40°, in good agreement with experiments.

The radii of the $K_\alpha$ spot obtained by simulations are compared with experiments in Figure 5. Simulations with the energy-dependent angular distribution reproduce quite well the effective propagation angle seen in the experiments, but present two differences with the experimental curve, namely: (1) the computed $K_\alpha$ spot radii are, approximately, 30 $\mu$m below experiments for all thicknesses; and (2) the almost constant $K_\alpha$ spot size found in simulations for targets thinner than 50 $\mu$m due to the beam collimation. These two differences can be reduced by using a fast electron source larger than the laser focal spot. This assumption is supported by the experimental results depicted in Figure 5, which show $K_\alpha$ radii much larger than the laser spot for targets as thin as 10 $\mu$m. Therefore, we increased the radius of the fast electron source with the limitation that the temperature at the target rear surface has to be similar to the temperature measured in the experiments, as will be explained in Section 3.3. With the parameters used here, we found a good agreement between simulations and experiments on this temperature when the laser focal spot is multiplied by a factor of 2.5, resulting in a fast electron source radius of 12.5 $\mu$m (FWHM) instead of the 5 $\mu$m of the laser spot. Fast electrons are injected into this "extended" source with a kinetic energy and an impinging angle that depend on the local laser intensity at the 5 $\mu$m focal spot, but with a radius 2.5 times larger. This is equivalent to assume a radial drift or lateral transport of fast electrons in the plasma at the target front side from the laser spot to the fast electron spot. Notice that this radial drift is more important for low energy electrons generated at the outermost zones of the laser spot. Stephens *et al*. (2004) pointed out some plausible physical mechanisms that can induce this lateral transport. Indeed, this effect was studied by a number of authors more

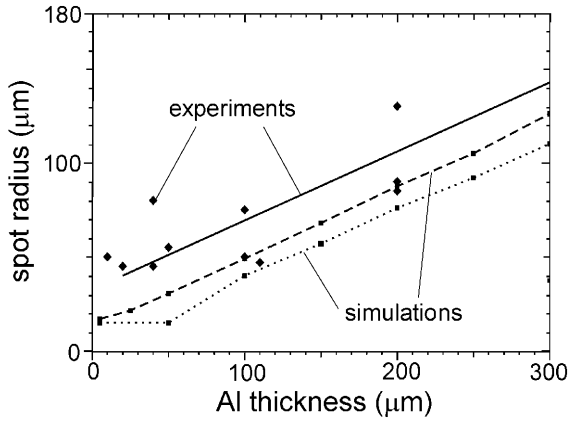


**Fig. 5.** Spot radius of the $K_\alpha$ photons emitted by the Al fluor layer as a function of the thickness of the Al transport layer. The dotted line corresponds to 5 $\mu$m fast electron spot radius at the front surface and the dashed line to 12.5 $\mu$m.

https://doi.org/10.1017/S0263034606060319 Published online by Cambridge University Press

than 20 years ago (Fabro & Mora, 1982; Forslund & Brackbill, 1982). However, since a theory to explain quantitatively the radial drift observed in current high-intensity experiments has not been developed yet, the increase of the size of the fast electron source used here can be considered as a fitting of our simulations to the experimental results. Simulations show (see Fig. 5) that when this "extended" source is used, the computed $K_\alpha$ radii increase, approximately, the same amount that the fast electron source, reducing the difference between computed and experimental $K_\alpha$ radii from 30 to 20 $\mu$m for almost all thicknesses. This is in agreement with the predictions of the analytical model of Bell and Kingham (2003) about the weak dependence of the self-generated azimuthal magnetic field ($\propto R^{-3/5}$), the beam collimation parameter ($\propto R^{2/5}$) and then the effective propagation angle on the beam radius $R$.

### 3.2. $K_\alpha$ yield

The computed $K_\alpha$ yields of the aluminum fluor layer are depicted in Figure 6. The experimental points have been plotted for comparison. The electron range obtained from simulations is 260 $\mu$m (for target thicknesses from 100 to 250 $\mu$m), in good agreement with the range of 250 $\mu$m measured in the experiments (Martinolli *et al*., 2003). The details of the radial distribution of the $K_\alpha$ photons are shown in Figure 4.

As was pointed out in previous calculations (Honrubia *et al*., 2004), the yield of the $K_\alpha$ photons with target thickness depends, to a large extent, on electron refluxing. In these calculations, we used fast electron reflection at the rear surface, free boundary at the front surface and found that $K_\alpha$ yield of 520 keV electrons can be fitted as a function of the thickness $z$ of the aluminum transport layer as $\exp(-z/z_0)$, where $z_0 = 300$ $\mu$m is the so-called "effective range." Here, the mean energy is higher (1.5 MeV), but the effective range is even lower (260 $\mu$m) due to the full refluxing used in the present calculations, which reduces this "effective range" or attenuation of the $K_\alpha$ yield with target thickness, as discussed in Honrubia *et al*. (2004).

### 3.3. Target heating

Target heating is mainly due to the resistive energy dissipation or Ohmic heating by the plasma return current. This mechanism heats the plasma up to keV temperatures in the first tens of $\mu$m. At higher depths, self-generated fields are less important and plasma temperatures are much lower, reaching approximately 30 eV at 100 $\mu$m depth and of 3–4 eV at 300 $\mu$m, as shown in Figure 7. It is also remarkable in this figure, the separation between collimated and non-collimated zones in the transport layer, and the width of the radial temperature profile at the rear side, which is in good agreement with the $K_\alpha$ radial distribution shown in Figure 4.

In spite that fast electrons have an important initial divergence, which in turn leads to smaller current densities and self-generated fields, the energy transferred to the plasma by Ohmic heating is a significant fraction of the fast electron pulse energy. For instance, in the case of the target with 100 $\mu$m aluminum transport layer, 16.5% of the energy carried by fast electrons is deposited by Ohmic heating. Thus, self-generated fields have to be taken into account even in large beam divergence cases.

Since we have assumed full refluxing in the present calculations, fast electrons pass through the target until they deposit all their energy. The balance between the energy deposited by Coulomb collisions with the background plasma and the Ohmic heating due to the return current is shown as a function of the target thickness in Figure 8. Notice that less than 18% of the fast electron pulse energy is deposited as Ohmic heating. This is almost a factor of 2 lower than the energy deposited when a Gaussian distribution with an initial divergence angle of 20° (FWHM) is used (Honrubia *et al*., 2004).

The temperature distribution at the target rear surface was measured for bare aluminum targets without fluor layers

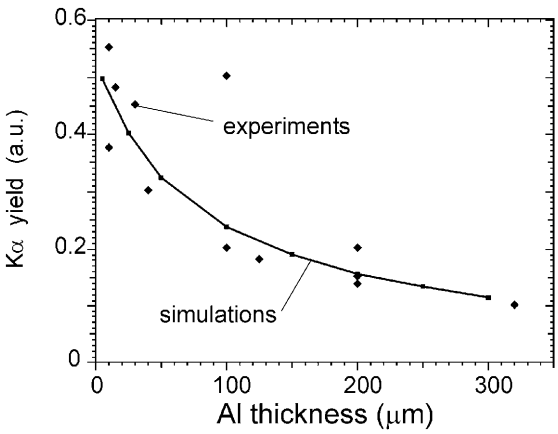


**Fig. 6.** $K_\alpha$ yield of the Al fluor layer as a function of the thickness of the Al transport layer in the target shown in Figure 2.

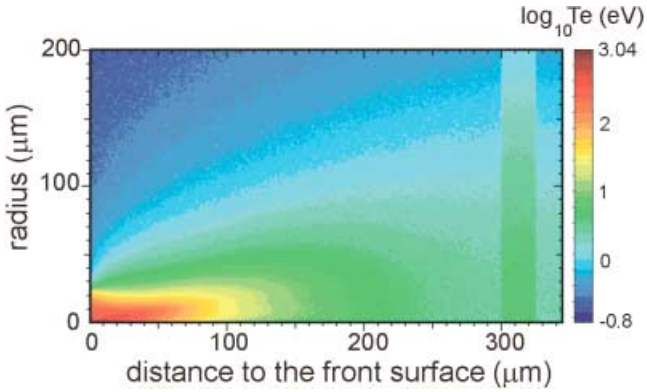


**Fig. 7.** Temperature distribution of the 300 $\mu$m target shown in Figure 2, 10 ps after the end of the laser pulse. Fast electrons are injected at the left of the simulation box.

https://doi.org/10.1017/S0263034606060319 Published online by Cambridge University Press

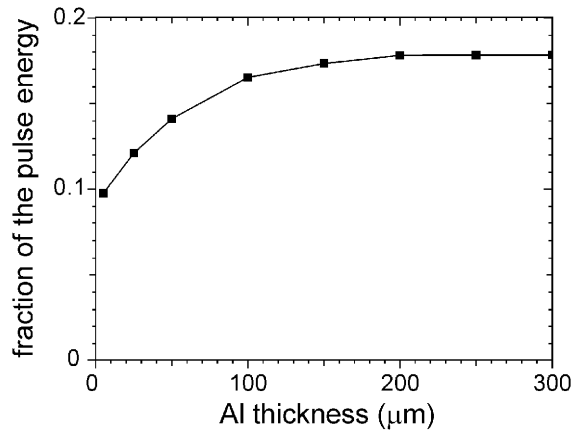


**Fig. 8.** Relative importance of the Ohmic heating in the targets sketched in Figure 2.

(Key *et al*., 2004; Stephens *et al*., 2004). We have performed simulations of these targets with the same parameters used in the former cases in order to compare our simulations with the experiments. The temperature profile at the rear surface of a 100 $\mu$m aluminum target is depicted in Figure 9. The peak temperature is 31 eV, and the FWHM of the spot 60 $\mu$m, close to the temperature of 30 eV and the spot of 70 $\mu$m measured in the experiments. This good agreement between simulations and experiments can be explained by the energy-dependent angular distribution of fast electrons used and confirms that the temperature overestimations typical of the hybrid PIC codes are due to an excessive collimation of the fast electron beam.

## 4. CONCLUSIONS

The main advantage of the hybrid PIC modeling as developed by Davies (2002) and Gremillet *et al*. (2002) is the large space and time scales that can be simulated with these codes with a reasonable computational cost. However, the full exploitation of this advantage has been hampered until now by the discrepancies found by several authors between predictions of these codes and the results of $K_\alpha$ experiments. Here, we found that using a suitable initial angular distribution of fast electrons and fitting the size of the fast electron source, hybrid PIC simulations can almost fully reproduce simultaneously for the first time the three independent diagnostics used in the experiments analyzed, namely divergence angle, $K_\alpha$ yield and temperature at the target rear surface. However, a theory to explain and predict the radial drift of fast electrons at the target front side as a function of the laser beam parameters is needed to determine in general the size of the fast electron source.

To have a well characterized fast electron source is important not only for simulation of $K_\alpha$ experiments, but also in other applications such as proton acceleration at the target rear surface, where resistive collimation of fast electrons determines to a large extent proton spectra.

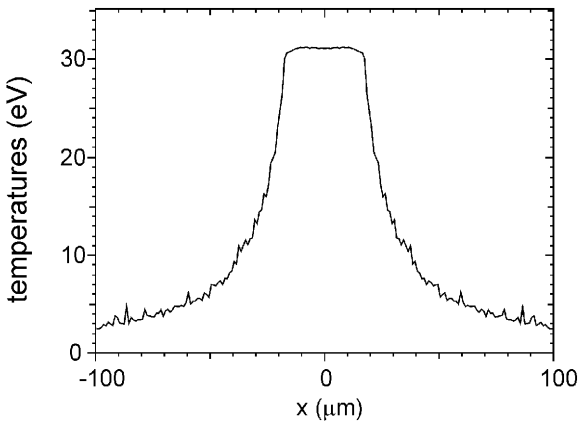


**Fig. 9.** Temperature profile at the rear surface of a 100 $\mu$m single layer Al target 10 ps after the end of the laser pulse.

## ACKNOWLEDGMENTS

This work has been supported by the research grant FTN2003-06901 of the Spanish Ministry for Education and Science and the "keep-in-touch" activities of EURATOM.

## REFERENCES

Alonso, L. (2003). Simulación y análisis de experimentos de propagación de electrones rápidos. MS Thesis. Madrid: Polytechnic University.

Baton, S.D., Santos, J.J., Amiranoff, F., Popescu, F.H., Gremillet, L., Koenig, M., Martinolli, E., Guilbaud, O., C. Rousseaux, C., Rabec Le Gloahec, M., Hall, T., Batani, D., Perelli, E., Scianitti, F. & Cowan, T.E. (2003). Evidence of ultrashort electron bunches in laser-plasma interactions at relativistic intensities. *Phys. Rev. Lett.* **91**, 105001.

Bell, A.R. & Kingham, R.J. (2003). Resistive collimation of electron beams in laser-produced plasmas. *Phys. Rev. Lett.* **91**, 035003.

Bibi, F.A., Matte, J.P. & Kieffer, J.C. (2004). Fokker-Planck simulations of hot electron transport in solid density plasma. *Laser Part. Beams* **22**, 97.

Davies, J.R. (2002). How wrong is collisional Monte Carlo modeling of fast electron transport in high-intensity laser-solid interactions? *Phys. Rev. E* **65**, 026407.

Eidmann, K., Meyer-ter-Vehn, J., Schlegel, T. & Hüller, S. (2000). Hydrodynamic simulation of subpicosecond laser interaction with solid-density matter. *Phys, Rev. E* **62**, 1202.

Evans, R.G., Clark, E.L., Eagleton, R.T., Dunne, A.M., Edwards, R.D., Garbett, W.J., Goldsack, T.J., James, S., Smith, C.C., Thomas, B.R., Clarke, R., Neely, D.J. & Rose, S.J. (2005). Rapid heating of solid density material by a petawatt laser. *Appl. Phys. Lett.* **86**, 191505.

Fabro, R. & Mora, P. (1982). Hot electrons behavior in laser-plane target experiments. *Phys. Lett.* **90A**, 48.

Fill, E. (2001). Relativistic electron beams in conducting solids and dense plasmas: Approximate analytical theory. *Phys. Plasmas* **8**, 1441.

https://doi.org/10.1017/S0263034606060319 Published online by Cambridge University Press

Forslund, D.W. & Brackbill, J.U. (1982). Magnetic-field-induced surface transport on laser-irradiated foils. *Phys. Rev. Lett.* **48**, 1614.

Gremillet, L., Amiranoff, F., Baton, S.D., Gauthier, J.C., Koenig, M., Martinolli, E., Pisani, F., Bonnaud, G., Lebourg, C., Rousseaux, C., Toupin, C., Antonicci, A., Batani, D., Bernardinello, A., Hall, T., Scott, D., Norreys, P., Bandulet, H. & Pépin, H. (1999). Time-resolved observation of ultrahigh intensity laser-produced electron jets propagating through transparent solid targets. *Phys. Rev. Lett.* **83**, 5015.

Gremillet, L., Bonnaud, G. & Amiranoff, F. (2002). Filamented transport of laser-generated relativistic electrons penetrating a solid target. *Phys. Plasmas* **9**, 941.

Honrubia, J.J., Antonicci, A. & Moreno, D. (2004). Hybrid simulations of fast electron transport in conducting media, *Laser Part. Beams* **22**, 129.

Honrubia, J.J., Kaluza, M., Schreiber, J., Tsakiris, G.D. & Meyer-ter-Vehn, J. (2005). Laser-driven fast-electron transport in preheated foil targets. *Phys. Plasmas* **12**, 052708.

Kemp, A.J. & Meyer-ter-Vehn, J. (1998). An Equation of state code for hot dense matter, based on the QEOS description. *Nucl. Inst. Meth. Phys. Res. A* **415**, 674.

Key, M.H., Amiranoff, F., Andersen, C., Batani, D., Baton, S.D., Cowan, T., Fisch, N., Freeman, R., Gremillet, L., Hall, T., Hatchett, S., Hill, J., King, J., Kodama, R., Koch, J., Koenig, M., Lasinski, B., Langdon, B., Mackinnon, A., Martinolli, E., Norreys, P., Parks, P., Perelli-Cippo, E., Rabec Le Gloahec, M., Rosenbluth, M., Rousseaux, C., Santos, J.J., Scianitti, F., Snavely, R., Tabak, M., Tanaka, K., Town, R., Tsutumi, T. & Stephens, R. (2004). Studies of electron transport and isochoric heating and their applicability to fast ignition. In *Inertial Fusion Sciences and Applications* (Hammel, B.A., Meyerhofer, D.D., Meyer-ter-Vehn, J. and Azechi, H., Eds.), p. 353. La Grange Park, IL: American Nuclear Society.

Koch, J.A., Key, M.H., Freeman, R.R., Hatchett, S.P., Lee, R.W., Pennington, D., Stephens, R.B. & Tabak, M. (2001). Experimental measurements of deep directional columnar heating by laser-generated relativistic electrons at near-solid density. *Phys. Rev. E* **65**, 016410.

Kodama, R., Norreys, P.A., Mima, K., Dangor, A.E., Evans, R.G., Fujita, H., Kitagawa, Y., Krushelnick, K., Miyakoshi, T., Miyanaga, N., Norimatsu, T., Rose, S.J., Shozaki, T., Shigemori, K., Sunahara, A., Tampo, M., Tanaka, K.A., Toyama, Y., Yamanaka,. T. & Zepf, M. (2001). Fast heating of ultrahigh-density plasma as a step towards laser fusion ignition. *Nature (London)* **412**, 798.

Martinolli, E., Koenig, M., Gremillet, L., Santos, J.J., Amiranoff, F., Baton, S.D., Batani, D., Scianitti, F., Perelli-Cippo, E., Hall, T.A., Key, M.H., Mackinnon, A.J., Freeman, R.R., Snavely, R.A., King, J.A., Andersen, C., Hill, J.M., Stephens, R.B., Cowan, T.E., Ng, A., Ao, T., Neely, D. & Clarke, R.J. (2003). Fast electron heating in ultra-intense laser-solid interaction using high brightness shifted $K_\alpha$ spectroscopy. Central Laser Facility Annual Report 2001/2002. CLRC, Chilton, U.K.

Martinolli, E., Koenig, M., Amiranoff, F., Baton, S.D., Gremillet, L., Santos, J.J., Hall, T.A., Rabec-Le-Gloahec, M., Rousseaux, C. & Batani, D. (2004). Fast electron heating of a solid target in ultrahigh-intensity laser pulse interaction. *Phys. Rev. E* **70**, 055402(R).

Quesnel B. & Mora, P. (1998). Theory and simulation of the interaction of ultraintense laser pulses with electrons in vacuum. *Phys. Rev. E* **58**, 3719.

Roth, M., Brambrink, E., Audebert, P., Blazevic, A., Clarke, R., Cobble, J., Cowan, T.E., Fernandez, J., Fuchs, J., Geissel, M., Habs, D., Hegelich, M., Karsch, S., Ledingham, K., Neely, D., Ruhl, H., Schlegel, T. & Schreiber, J. (2005). Laser accelerated ions and electron transport in ultra-intense laser matter interaction. *Laser Part. Beams* **23**, 95.

Santos, J.J., Amiranoff, F., Baton, S.D., Gremillet, L., Koenig, M., Martinolli, E., Rabec Le Gloahec, M., Rousseaux,, C., Batani, D., Bernardinello, A., Greison, G. & Hall, T. (2002). Fast electron transport in ultraintense laser pulse interaction with solid targets by rear-side self-radiation diagnostics. *Phys. Rev. Lett.* **89**, 025001.

Stephens, R.B. Snavely, R.A., Aglitskiy, Y., Amiranoff, F., Andersen, C., Batani, D., Baton, S.D., Cowan, T., Freeman, R.R., Hall, T., Hatchett, S.P., Hill, J.M., Key, M.H., King, J.A., Koch, J.A., Koenig, M., Mackinnon, A.J., Lancaster, K.L., Martinolli, E., Norreys, P., Perelli-Cippo, E., Rabec Le Gloahec, M., Rousseaux, C., Santos, J.J. & Scianitti, F. (2004). $K_\alpha$ fluorescence measurements of relativistic electron transport in the context of fast ignition. *Phys. Rev. E* **69**, 066414.

Tikhonchuk, V. (2002). Interaction of a beam of fast electrons with solids. *Phys. Plasmas* **9**, 1416.

Town, R.P.J., Chen, C., Cottrill, L.A., Key, M.H., Kruer, W.L., Langdon, A.B., Lasinski, B.F., Snavely, R.A., Still, C.H., Tabak, M., Welch, D.R. & Wilks, S.C. (2005). Simulations of electron transport for fast ignition using LSP. *Nucl. Instr. Meth. Phys. Res. A* **544**, 61.

Wilks, S.C., Kruer, W.L., Tabak, M. & Langdon, A.B. (1992). Absorption of ultra-intense laser pulses. *Phys. Rev. Lett.* **69**, 1383.